Prediction of acoustic resonance phenomena for weapon bays using detached eddy simulation

R. M. Ashworth
QinetiQ
Farnborough
UK

ABSTRACT

It is argued that acoustic resonance phenomena in open cavities such as weapons bays cannot be adequately predicted through numerical solution of Reynolds averaged Navier-Stokes (RANS) equations. The requirement to resolve the growth of the shear layer instability from the lip of the cavity inevitably implies that turbulence further downstream is resolved while also being modelled thus making RANS over dissipative. Large eddy simulation (LES) models only unresolved scales and a hybrid method combining RANS near walls with LES in the cavity appears a practical alternative to pure RANS. This paper compares computations of the M219 cavity configuration made with unsteady RANS and with the hybrid method known as detached eddy simulation (DES). It is shown that whilst unsteady RANS and DES give very similar predictions for the 1st and 3rd modes of the acoustic resonance the 2nd mode (which is dominant near the centre of the cavity) is absent in the RANS results but well predicted by DES. The 2nd mode is thought to arise from an interaction with vortical structures in the shear layer which are suppressed in the highly dissipative RANS method. The 4th mode, which is much weaker than the other three modes, is over-predicted by DES and under-predicted by a smaller amount in RANS.

NOMENCLATURE

D	depth of cavity
L	length of cavity
p_{ref}	reference pressure (minimum audible variation)
S_k	spectral density of turbulent kinetic energy
W	width of cavity
ϕ_f	value of flow variable on cell face
ϕ_f^{UP}	upwinded update for ϕ_f
ϕ_f^{CD}	central difference update for ϕ_f
μ_t	turbulent viscosity
μ_0	molecular viscosity
ω	angular frequency

Abbreviations

CFD	computational fluid dynamics
DES	detached eddy simulation
LES	large eddy simulation
PISO	pressure-implicit with splitting of operators
PSD	power spectral density
RANS	Reynolds averaged Navier-Stokes
rms	root mean square
URANS	unsteady RANS
SPL	sound pressure level

1.0 INTRODUCTION

Design requirements of modern combat aircraft include low radar cross section which can be met only if weapons carried by the aircraft are enclosed in a weapons bay within the airframe. Compared to external carriage this has the added benefit of significantly reducing drag. However there are significant problems associated with delivering weapons through the aggressive aerodynamic environment that results when the bay doors are opened. Of particular concern is aero-acoustic resonance which results in discrete tones containing high levels of energy[1]. These can exert severe damage on both the weapons and the surrounding aircraft systems.

The acoustic resonance phenomenon in 'open cavities' such as weapon bays arise from a feedback mechanism between the growth of shear layer instabilities from the cavity leading edge and the periodic impingement of high speed flow on the rear wall of the cavity.

Paper No. 2970. Received on 27 April 2005, revised copy received on 26 July 2005, accepted 1 November 2005.

https://doi.org/10.1017/S0001924000000968 Published online by Cambridge University Press

Pressure waves emanating from the latter trip the former leading to undulations in the shear layer with further high speed impingement on the rear wall. Empirical methods based on the pioneering work of Rossiter[2], are able to give reasonable predictions for the frequency of these resonances but have met with less success in predicting amplitudes.

In recent years there has been considerable interest in the possibility of using computational fluid dynamics (CFD) to accurately predict both the frequency and amplitudes of these resonances. The interest is not only in empty weapons bays but also in weapon bays with complex stores for which empirical methods have very little to offer. A proven CFD capability would enable rapid cavity prototype design including palliative measures (e.g. ramps and spoilers) to ameliorate the resonance phenomena.

Much of the recent effort has been directed to performing unsteady Reynolds averaged Navier-Stokes (unsteady RANS or URANS) computations for empty rectangular cavities as a preliminary to more challenging configurations. However, even at this simplest level it is found that whilst the frequencies of the resonant modes are often quite well predicted, the amplitude of the modes invariably are not.

The failings of URANS computations may be due to inappropriate application of the method or choice of turbulence model. However, it has also been suggested[3] that URANS methods are intrinsically unsuited to such flows due to an overlap between turbulence and convective scales with consequent double accounting of the turbulent energy drain.

More recent efforts have turned to large eddy simulation (LES) in which only the unresolved scales are modelled. This has met with considerable success in some cases e.g. (Refs 4,5) for the M219 cavity. However this approach is too computationally intensive to be of practical design value. Hybrid RANS/LES methods in which the LES is restricted to regions in which it is essential, offer a more affordable alternative. Increasing effort is now being directed towards the hybrid method first proposed by Strelets[6] and known as detached eddy simulation (DES).

This paper compares the use of URANS and DES for an empty rectangular cavity at Mach number 0·85 corresponding to the M219 configuration used in experiments by QinetiQ[7,8,9]. Some supporting evidence for the unsuitability of URANS for this particular configuration can be obtained through a spectral analysis of the LES data generated at ONERA and analysed in great detail in (Refs 4,5). QinetiQ has been able to obtain this data from ONERA and has reproduced some of the spectral analysis for points in the shear layer.

Figure 1 shows the kinetic turbulent energy spectrum for two of these points. The first is just downstream (5% of cavity length) of the lip and the second is further downstream (15% of cavity length). The peak at around 4kHz in the first plot is the energy associated with the growth of a Kelvin-Helmholtz instability. Turbulence levels at this point are still low. In the second plot it is seen that turbulence levels have grown with a turbulence cascade (indicated by the $\omega^{-5/3}$ inertial range scaling) starting at around 2kHz.

The requirement to resolve the growth of the shear layer instability at around 4kHz clearly implies a double accounting of the turbulence energy drain in URANS since scales associated with the former overlap with the latter. The cascade is both modelled and resolved.

The computations described here were made with the commercial solver, Fluent 6.1, on a common mesh for URANS and DES. Comparisons have been made between computational and experimental sound pressure levels (SPLs) and root mean square (rms) pressures at ten locations along the cavity ceiling. The results indicate a complete failure of URANS to predict one of the four resonance modes which is well predicted by DES. Dominance of this mode near the centre of the cavity makes its accurate prediction critical.

2.0 EXPERIMENTAL CONFIGURATION

The configuration (see Fig 2) consisted of a rectangular cavity cut into a flat plate of length 72 inches and width 17 inches. The depth (D) of the cavity was 4 inches, the width (W) was 4 inches and the length (L) was 20 inches giving the ratio $D:W:L$ = 1:1:5. The leading edge of the cavity was located 31 inches downstream from the plate leading edge and the cavity centre-line was off-set 1 inch from the rig centre-line.

Kulite pressure measurements were made with a frequency of 6kHz at a number of locations (see Fig. 3) including ten equally spaced points along the rig centre-line on the cavity ceiling. Pressure histories from these latter points were used in the comparison with computation described here.

3.0 COMPUTATION

3.1 Introduction

A detailed description of the DES model used in Fluent and the associated numerical scheme can be found in Ref. 10. These details are summarised with appropriate references in the sections below. The mesh design and choice of time-step (see below) has been based on the experience of M219 cavity computations reported in[11].

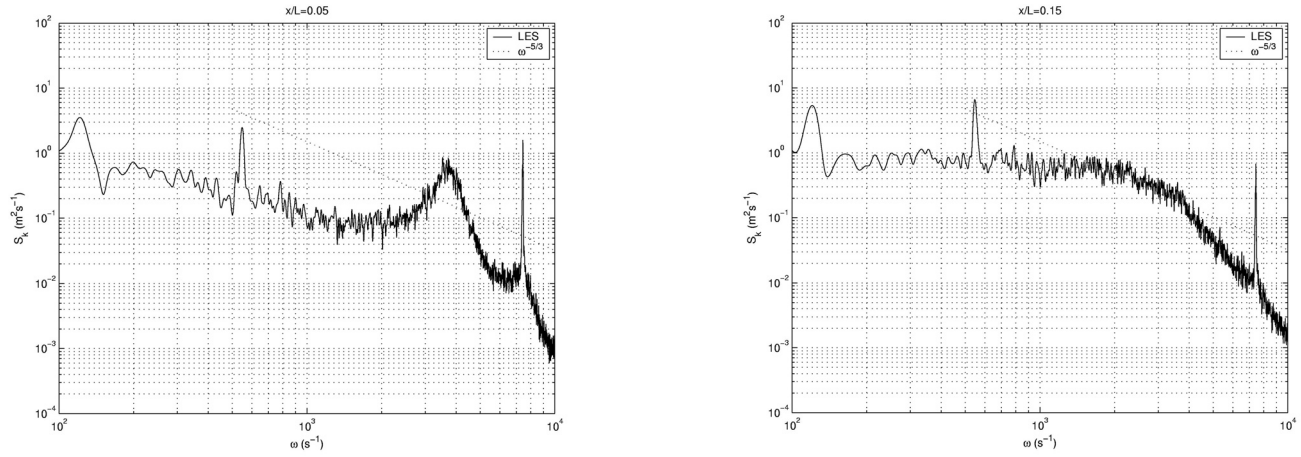


Figure 1. Turbulent kinetic energy density from ONERA LES in shear layer at 5% and 15% of cavity length downstream from lip.

https://doi.org/10.1017/S0001924000000968 Published online by Cambridge University Press

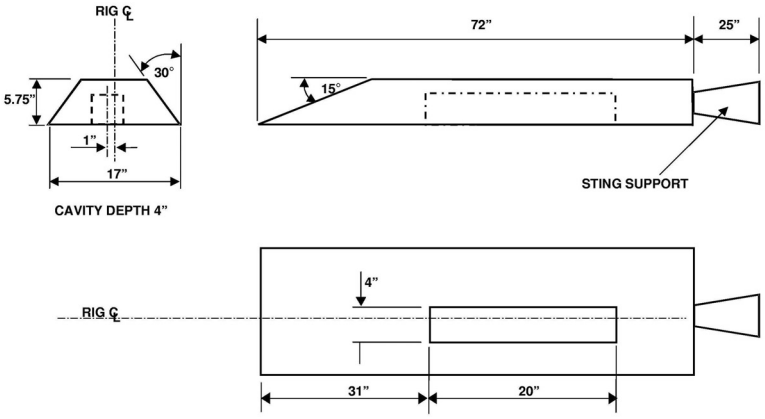
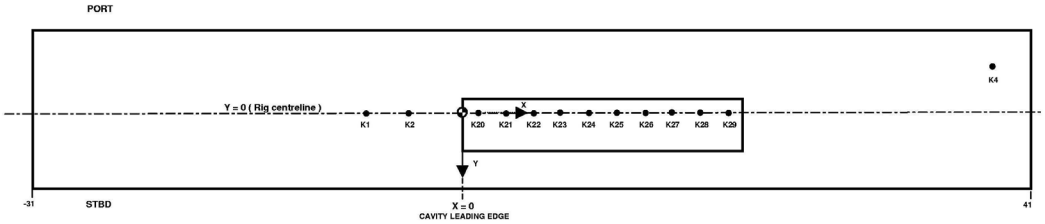
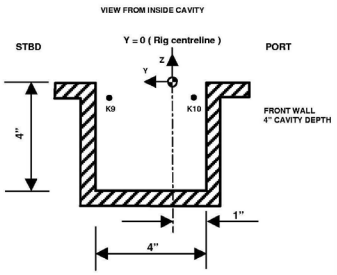


Figure 2. Cavity rig model.





Front plate	K1	-7.0		0.0	0.0
	K2	-4.0		0.0	0.0
Rear plate	K4	39.0		-3.0	0.0
4" Front wall	K9	0.0		2.5	-1.0
	K10	0.0		-0.5	-1.0
Ceiling	K20	1.0	0.05	For 4" cavity depth strip is located at Y=0" (ie not on cavity centreline)	
	K21	3.0	0.15		
	K22	5.0	0.25		
	K23	7.0	0.35		
	K24	9.0	0.45		
	K25	11.0	0.55		
	K26	13.0	0.65		
	K27	15.0	0.75		
	K28	17.0	0.85		
	K29	19.0	0.95		
Tunnel wall	K37	-	Port tunnel working section		

Figure 3. Kulite transducer positions.

3.2 Model

The DES computation was made with the Spalart-Allmaras DES model[12] that is available in Fluent. For the URANS comparison it might seem natural to have chosen the corresponding RANS turbulence model of Spalart-Allmaras[13]. However, this model is very over-dissipative in detached regions such as the shear layer over the cavity, due to the use of wall distance in the dissipation term of the viscosity transport equation. The DES model avoids this by switching to LES mode in detached regions. It was decided that a more sensible comparison would be with the SST version of Menter's hybrid k-ω/k-ε model[14]. This model combines the known benefits of Wilkox's k-ω model[15] for near wall regions with the known benefits of the standard k-ε[16] for wall remote shear layers and thus better represents

https://doi.org/10.1017/S0001924000000968 Published online by Cambridge University Press

the capabilities of RANS methods for this flow. The Fluent implementation of both the DES and RANS model includes automatic switching between low Reynolds number formulation and use of wall functions as appropriate according to first cell height.

3.3 Numerical scheme

For the DES a segregated cell centred finite volume scheme was used with second order implicit time integration and PISO pressure velocity coupling. A second order accurate central differencing scheme was used for the momentum equations in order to avoid the numerical dissipation of upwind schemes. The scheme is stabilised through the use of a deferred approach in which face values of variables, ϕ_f are calculated as the sum of an implicit upwind update and the difference between an explicit central difference update and an explicit upwind update,

$$\phi_f = \left[\phi_f^{UP}\right]_{\text{implicit}} + \left[\phi_f^{CD} - \phi_f^{UP}\right]_{\text{explicit}} \quad \ldots(1)$$

where UP stands for upwind and CD stands for central difference. This converges to a pure second order central difference update (see (Ref. 10) for further details).

For the URANS computations the numerical scheme was the same in all details except the last. The deferred central difference scheme was not available for URANS so a second order upwind scheme was used. Thus the higher levels of dissipation anticipated in the URANS computation cannot all be attributed to the greater eddy viscosity value.

3.4 Geometry and computational domain

The exact geometry of the experimental rig was approximated with a cavity in a plate of equal length to the rig and width anticipated to be sufficient to remove interference from side boundaries. In terms of the depth (D) of the cavity, the computation domain consisted of two cuboidal domains. The first of these was the interior of the cavity. The second was the volume bounded by the plane of the plate, an inflow plane corresponding to the leading edge of the rig (7·75D upstream of the cavity front wall), an outflow plane corresponding to the trailing edge of the rig (5·25D downstream of the cavity back wall), an upper boundary (17·0D above the cavity) and side boundaries (1·5D from the cavity centreline).

3.5 Boundary conditions

For both the DES and URANS computations pressure far field conditions were applied on the inflow, outflow and upper boundaries with Mach number M = 0·85, pressure P = 62940Pa, temperature T = 270·25K and eddy viscosity ratio $\mu_t/\mu_0 = 10$. Adiabatic wall conditions were applied on the plane of the plate and the cavity walls. Ideally non-reflective boundary conditions would have been applied at the side boundaries. However, these were not available for Fluent's segregated scheme. Thus symmetry conditions were applied on the side boundaries with the expectation from work elsewhere (e.g.(Ref. 11)) that the boundaries would be remote enough to avoid any significant interference effects. Initial conditions for the DES were obtained from a steady RANS computation with the Spalart Allmaras model.

3.6 Time integration

A time-step of 2×10^{-5} seconds was selected with a maximum of 30 iterations per time-step. The computation was run for a total of 25,000 time-steps or 0·5 seconds real time. While DES computations required the full 30 iterations to achieve adequate convergence with-in each time-step, URANS converged in less than half the number of iterations and hence completed the computation in less than half the time.

3.7 Mesh

The mesh was designed to have a similar level of refinement in and around the cavity as good as or better than that used in one of the more successful DES computations of the M219 cavity in existence at the time of commencement of this work[11].

The meshing strategy was to start with a 10 block structured mesh having isotropic (unit aspect ratio) cells in the interior of the cavity and high aspect ratio cells near walls. This was then imported into Fluent and refined in the shear layer and incoming boundary layer through $2 \times 2 \times 2$ splitting of hexahedral cells giving an unstructured mesh with hanging nodes (see Figs 4 and 5). In this way it was possible to avoid having as many points in the free-stream as the highly resolved shear layer would otherwise imply.

The distribution of points in the mesh was such that of the 1·68m total number of cells about 0·42m cells were within the highly

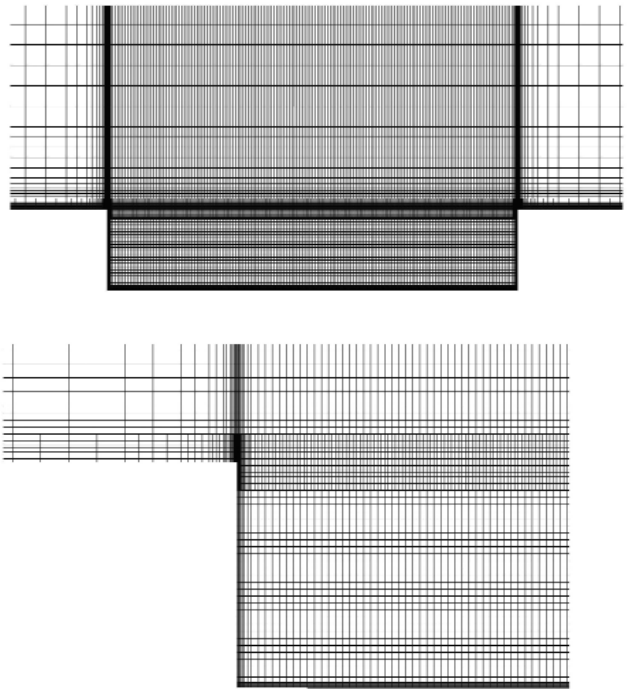


Figure 4. Stream-wise section of mesh (above) and detail (below).

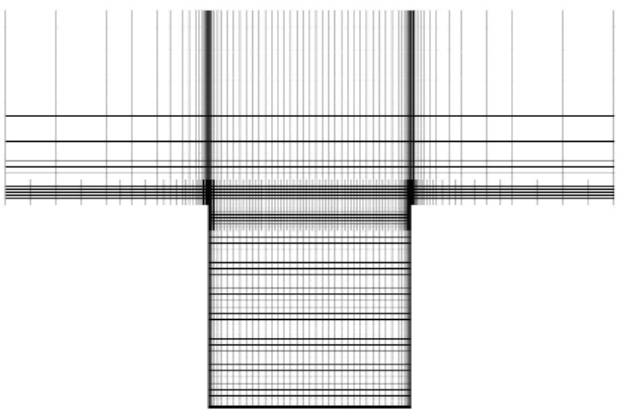


Figure 5. Span-wise section of mesh.

https://doi.org/10.1017/S0001924000000968 Published online by Cambridge University Press

refined shear layer region at the opening of the cavity and a further 0·43m cells in the remainder of the cavity. There were approximately eight points spanning the vorticity thickness at the lip of the cavity. The mesh was designed to be of wall function type on the plate surrounding the cavity and of low Reynolds number type on the cavity walls.

4.0 POST PROCESSING

4.1 Power spectral densities

The first 0·1s of computational pressure history was discarded to eliminate any transients leaving 0·4s of pressure history at a sampling frequency of 50kHz. For experiment 3·2s of the pressure history were used with a sampling frequency of 6kHz.

Computational power spectral densities (PSDs) were computed from the 0·4s of data. Experimental PSDs were computed both from the entire 3·2s of pressure data and from successive intervals of 0·4s. Any variation between the latter would indicate some uncertainty in the validity of stopping the computation at 0·4s.

The PSDs were computed with MATLAB using Welch's method of averaging over periodograms[17]. Blocks of 0·1s duration were used with a 50% overlap between blocks. Results were plotted in terms of sound pressure levels (SPLs) related to the PSD by

$$\mathrm{SPL} = 10\log(\mathrm{PSD}/\ p_{\mathrm{ref}}^2) \qquad \ldots(2)$$

where ,

$p_{\mathrm{ref}} = 20\,\mathrm{mPa}$

is the minimum audible pressure variation.

The effect of different sampling frequencies for experiment and computation is to give different upper (Nyquist) frequency limits for the spectra (3kHz and 25kHz respectively). This has no implications for comparisons of PSD within the common frequency range. However, root mean square pressure variations are derived by summing PSD over frequencies and a proper comparison should ensure that this summation is over the same range (here taken to be the experimental range).

5.0 RESULTS

5.1 Sound pressure levels

Figure 6 shows the SPL at all ten kulite locations. The first thing to be noticed is that there is a spread of about 5dB in the experimental SPL for different 0·4s intervals with the SPL for 3·2s positioned near the midpoint of the range. This casts uncertainty on the validity of stopping the computation at 0·4s unless it can be explained how some approximation in the computation serves to average out the longer time variations seen in experiment.

Comparing DES and URANS the most obvious difference is the complete failure to predict the second mode in the URANS computation. The first and third modes are very similar in the two methods but the fourth mode is much weaker in the URANS computation. Broadband noise is lower in the URANS computation.

Comparing the DES computation against experiment (for 3·2s), The level of the first mode is least well predicted with an over-prediction ranging from 6 to 12dB. The second mode is rather well predicted with an under-prediction ranging from less than 1 to 4dB. The third mode is over-predicted by an amount in the range 4 to 7dB and the fourth mode is also over-predicted by an amount in the range 2 to 7dB. Resonance frequencies are very well predicted for the first mode (with-in 10Hz), quite well for the second and third modes (with-in 30kHz) and not so well for the much weaker fourth mode (less than 50Hz).

5.2 Root mean square pressure

Root mean square (rms) pressure variations derived from summing PSD over the experimental frequency range are shown for all ten kulite locations in Fig. 7. It is seen that the experimental results display a variation ranging up to 400Pa from successive 0·4s intervals. The largest deviation between URANS and DES occurs near the centre of the cavity where the 2nd mode becomes dominant. This is virtually absent in the URANS computation thus accounting for the lower rms pressure variation here. The DES appears to give the right shape for the rms pressure variation but over-predicts the level by an amount in the range 800-1,200Pa. The greatest % error occurs near the front of the cavity where the rms pressure variation is lower.

5.3 Band limited rms pressures

More information about the contribution of different modes to the rms pressure variation can be gleaned by summing the PSD over a band of frequencies surrounding that of the resonance modes. This has been done for the following four bands corresponding to each of the four modes;

Band 1: 50-250Hz
Band 2: 300-500Hz
Band 3: 500-700Hz
Band 4: 750-900Hz.

The resulting rms pressure plots are shown in Fig. 8. It can be seen that there is a significant variation in the 0·4 seconds experimental rms pressure for all modes, particularly towards the rear of the cavity.

The URANS and DES results are similar for the 1st mode except near the front and rear of the cavity where the URANS results show a greater over-prediction due to the existence of additional lower frequency peaks in the URANS SPL spectrum.

The 3rd mode predictions for URANS and DES are almost indistinguishable from each other consistent with what is seen in the SPL spectra. For the much weaker 4th mode URANS and DES give similar shape to each other and experiment with a slight under-prediction compared to experiment for URANS and a larger over-prediction compared to experiment for DES.

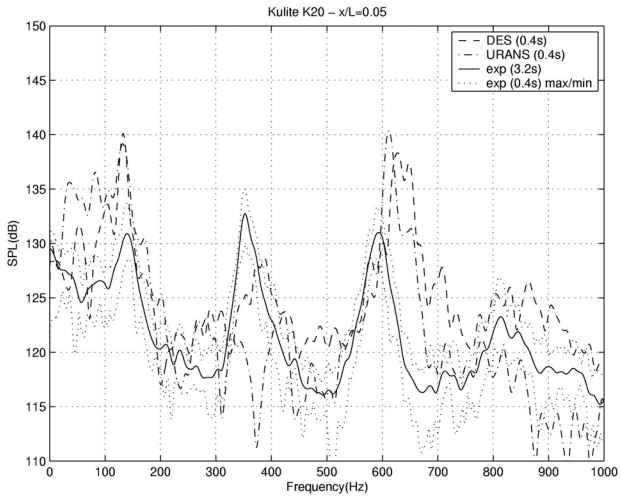
The most significant difference between URANS and DES is in the 2nd mode predictions. Whilst this mode is very well predicted in the DES results it is completely absent in the URANS results.

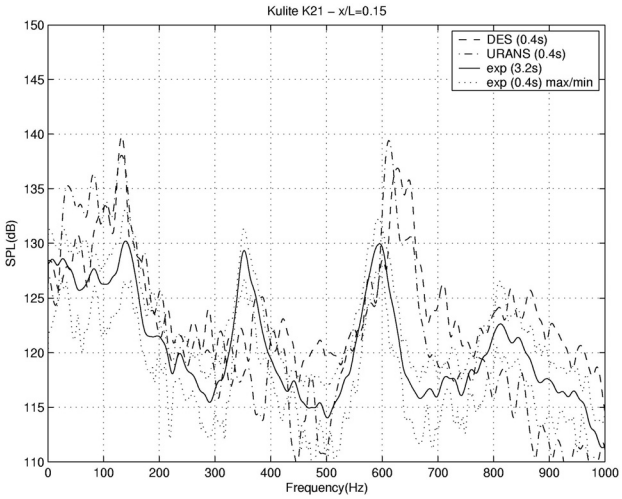
5.4 Convergence in computational PSD

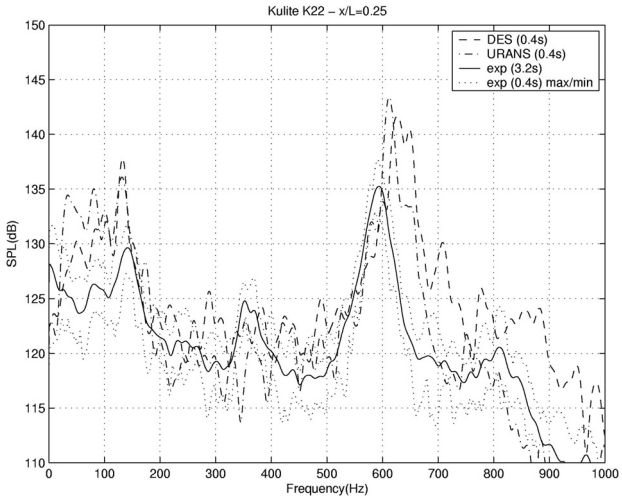
The spread in experimental results taken from successive 0·4 seconds intervals suggests that a 0·4 second computation may not be adequate. As a further indication regarding this rms pressures were computed from 0·1, 0·2, 0·3 and 0·4s intervals of post transient pressure history from the DES. The results are shown in Fig. 9.

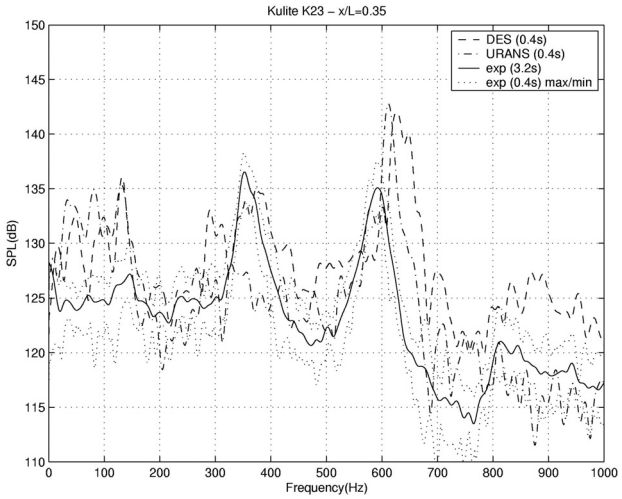
It is seen that there is a significant change everywhere except for the three kulites nearest the front of the cavity and the kulites at x/L=0·55. For the remaining kulites the changes becomes small only after 0·3s and it appears that adequately converged results are obtained everywhere for a pressure history of 0·4s duration.

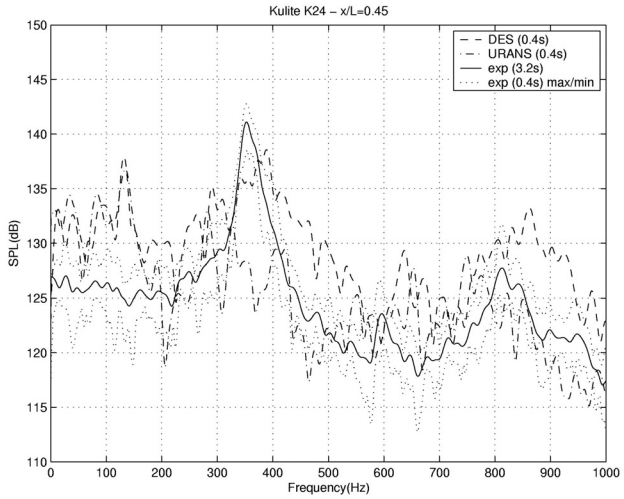
https://doi.org/10.1017/S0001924000000968 Published online by Cambridge University Press

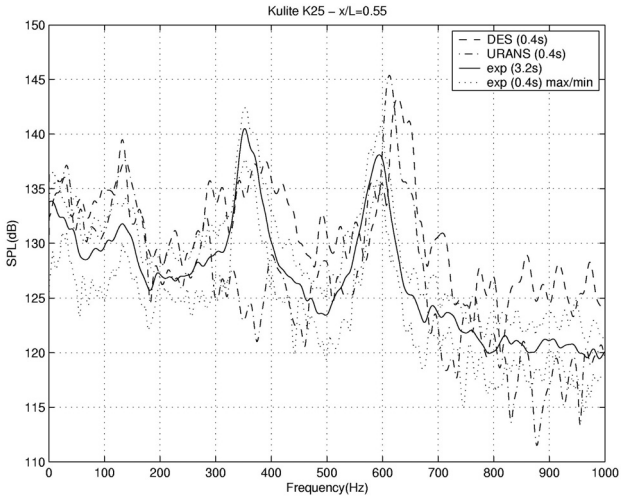












https://doi.org/10.1017/S0001924000000968 Published online by Cambridge University Press

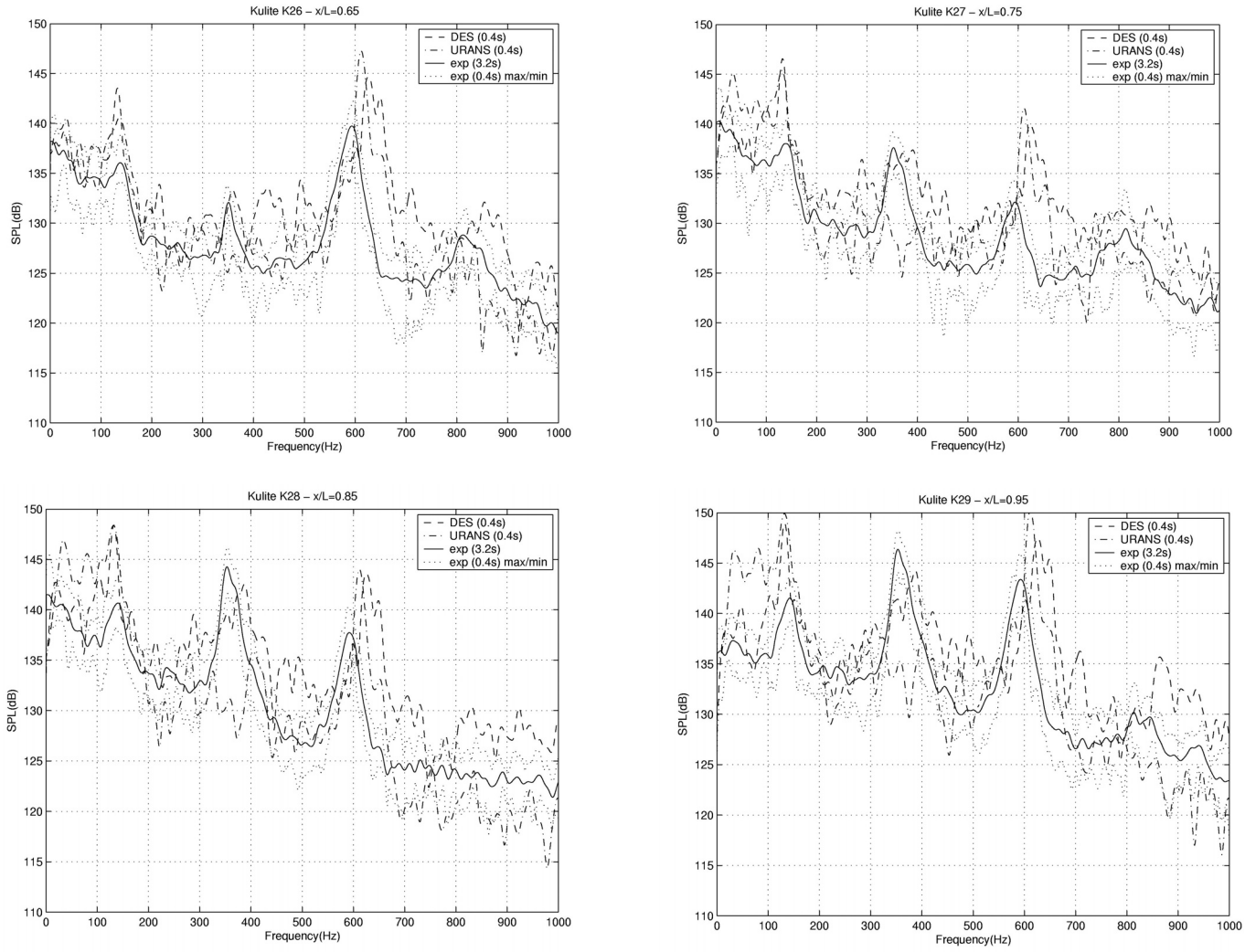


Figure 6. SPL at kulites on cavity ceiling.

5.5 Vorticity magnitude on symmetry plane

Figure 10 shows contours of vorticity magnitude on the symmetry plane of the cavity for the DES and URANS computations. This reveals quite clearly the much more detailed level of turbulence structure captured by the DES which is lost through the action of the excessive eddy viscosity and more dissipative numerical scheme in the URANS simulation.

6.0 CONCLUSIONS

For the doors-off M219 open cavity configuration considered in this paper, DES and URANS perform similarly in predicting the 1st and 3rd modes but URANS fails completely to predict the 2nd mode while DES seems particularly successful in predicting this mode. The much weaker 4th mode is slightly under-predicted by URANS and over-predicted by DES.

The 3rd mode is associated with the periodic propagation of an acoustic wave upstream from the rear cavity wall following impingement of high velocity fluid due to streamwise undulations in the shear layer. This process does not seem to be very critically affected by the accurate resolution of vortical structures.

The 1st mode appears to be a modulation in the intensity of these acoustic waves arising from spanwise undulations in the shear layer and is likewise not much affected by the accurate resolution of vortical structures.

The 2nd mode, which most clearly highlights the difference between URANS and DES, arises from the interaction with the vortices in the shear layer being convected downstream. It is known that this can be satisfactorily captured by URANS for the doors-on M219 configuration[11] which is much more two dimensional in character.

In the highly three dimensional doors-off case examined here the vortices are stretched and twisted through the spanwise ingress and egress of fluid above the surrounding plate which in turn is driven by the periodic pressure variation induced by the passing vortices. It seems probable that it is necessary to capture the details of this process which results in the break-up of larger vortices and generation of smaller vortical structures in order to properly capture the 2nd mode. It is suggested that URANS failure to capture this process, evident in Fig. 11, is largely due to its over-dissipative character in regions where convective and turbulence scales overlap (though the role of numerical dissipation remains to be clarified).

ACKNOWLEDGEMENTS

This work was funded under Weapon and Platform Effectors Domain of the UK MoD Research Programme.

https://doi.org/10.1017/S0001924000000968 Published online by Cambridge University Press

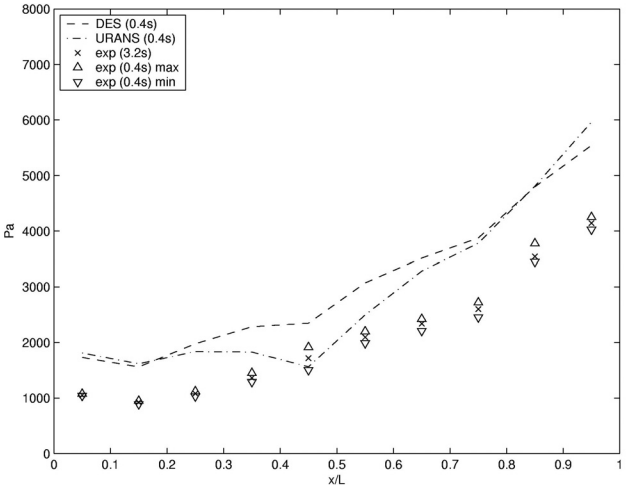


Figure 7. Root mean square pressure along cavity ceiling.

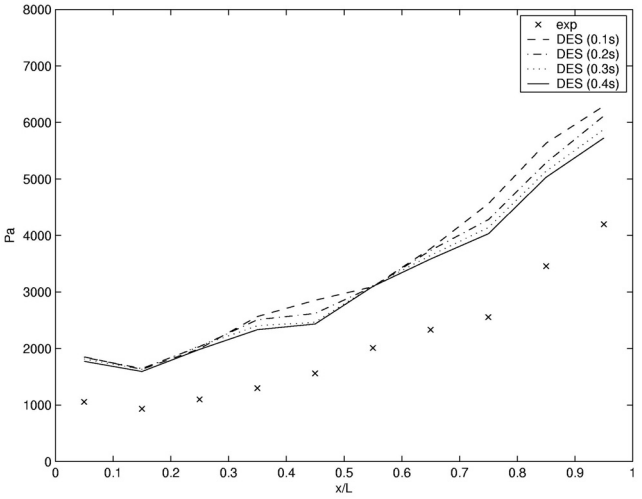


Figure 9. Effect of pressure history duration on rms pressure.

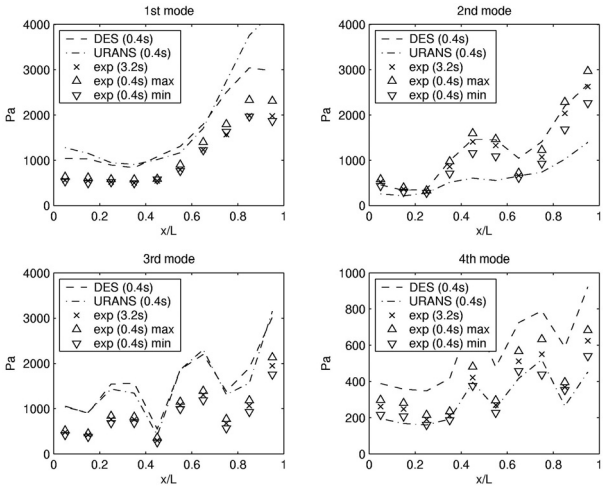


Figure 8. Band limited rms pressure along cavity ceiling.

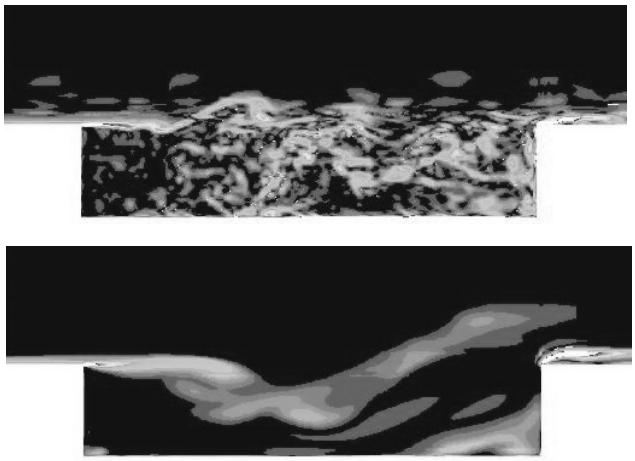


Figure 10. Contours of vorticity magnitude in symmetry plane for DES (top) and URANS (bottom).

REFERENCES

1. FORESTIER, N., JACQUIN, L. and GEFFROY, P. The mixing layer over a deep cavity at high subsonic speed, *J Fluid Mech*, 2003, 475, pp 101-145.
2. ROSSITER, J.E. Wind tunnel experiments on the flow over rectangular cavities at subsonic and transonic speeds, 1964, Aeronautical Research Council Reports and Memoranda 3438, London.
3. SINHA, D., DASH, S.M., CHIDAMBARAM, N. and FINDLAY, D. A perspective on the simulation of cavity aeroacoustics, AIAA-98-0286.
4. LARCHEVEQUE, L., SAGAUT and P. LÊ, T-H, Large-eddy simulations of flows in weapon bays, AIAA 2003-0778.
5. LARCHEVEQUE, L., SAGAUT, P. LÊ, T-H and COMTE, P. Large-Eddy Simulation of a compressible flow in a three-dimensional open cavity at high Reynolds number, under considerations for publication in *J Fluid Mech.*
6. STRELETS, M. Detached eddy simulation of massively separated flows, 2001, AIAA paper, 2001-0879.
7. STANEK, M.J., RAMAN, G., KIBENS, V., ROSS, J.A., ODEDRA, J. and PETO, J.W. Control of cavity resonance through very high frequency forcing, 2000, AIAA paper, 2000-1905.
8. STANEK, M.J., RAMAN, G., KIBENS, V., ROSS, J.A., ODEDRA, J. and PETO, J.W. Suppression of cavity resonance using high frequency forcing — the characteristic signature of effective devices, 2001, AIAA paper, 2001-2128.
9. HENSHAW, M.J. de C., 'M219 cavity case' in 'Verification and validation data for computational unsteady aerodynamics', Tech Rep RTO-TR-26, AC/323(AVT)TP/19, pp 453-472.
10. COKLJAT D. and LIU, F. DES of turbulent flow over an airfoil at high incidence, 2002, AIAA paper, 2002-0590.
11. MENDONÇA, F., ALLEN, R., CHARENTENAY, J. and KIRKHAM, D., CFD prediction of narrowband and broadband cavity acoustics at M = 0·85, 2003, AIAA paper, 2003-3303.
12. SPALART, P.R., JOU W.H., STRELETS, M. and ALLMARAS, S.R. Comments on the feasibility of LES for wings and on a hybrid RANS/LES approach, Proceedings of the first AFOSR conference on DES/LES, edited by LIU, C. and LIU, Z. (Eds), Greyden Press.
13. SPALART, P.R. and ALLMARAS, S.R. A one-equation turbulence model for aerodynamic flows, 1992, AIAA paper 92-0439.
14. MENTER, F.R. Zonal two-equation k-ω turbulence models for aerodynamic flows, 1993, AIAA paper 93-2906.
15. WILCOX, D.C., Reassessment of the scale determining equation for advanced turbulence models, *AIAA J,* 1988, **26,** pp 1299-1310.
16. JONES, W.P. and LAUNDER, B.E., The calculation of low Reynolds number phenomena with a two equation model of turbulence, *Int J Heat Mass Transf, 1973,* **16,** pp 1119-1130.
17. WELCH, P.D. The use of fast Fourier transform for the estimation of power spectra, June 1970, IEEE Trans Audio Electroacoustics, AU-15, pp 70-73.

https://doi.org/10.1017/S0001924000000968 Published online by Cambridge University Press